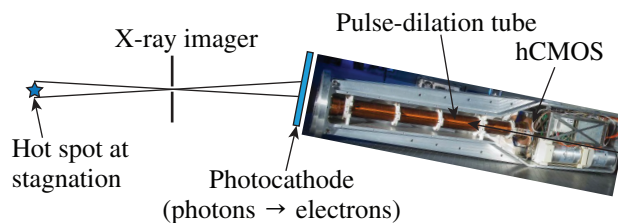


The Single-Line-of-Sight, Time-Resolved X-Ray Imager Diagnostic on OMEGA

Introduction

Time-resolved x-ray imaging of the self-emission from a hot spot formed in implosions of cryogenic deuterium–tritium (DT) shells in inertial confinement fusion experiments provides critical information for inferring the hot-spot pressure.¹ A 16-channel, framing-camera–based, time-resolved Kirkpatrick–Baez x-ray microscope (KBframed)² is routinely used to measure the evolution of the stagnation region of imploded cryogenic targets on the University of Rochester’s OMEGA Laser System.³ The high spatial ($\sim 6\text{-}\mu\text{m}$) and temporal ($\sim 40\text{-ps}$) resolutions of this system make it possible to accurately determine the core emission size and shape at the peak of stagnation. The hot spot in OMEGA implosions typically has a radius of ~ 20 to $30\ \mu\text{m}$, and the core x-ray emission lasts for $\sim 100\ \text{ps}$ (Ref. 2). Measurements of the core size, ion temperature, neutron-production temporal width, and neutron yield provide the input to infer the hot-spot pressure, which currently exceeds 50 Gbar in OMEGA implosions.¹ Multiple-lines-of-sight imaging will provide information about the hot-spot morphology and improve the confidence in the measurement of its size. This is important to better understand the physics that currently limits the hot-spot pressure. The new diagnostics will contribute to strategies to improve the implosion performance so that pressures are reached that will scale to ignition-relevant implosions. With the achievable target compression on OMEGA, the optimum photon-energy range for imaging the hot spot is 4 to 8 keV, where the shell is optically thin to this radiation. This article discusses a novel time-gated, x-ray imager that was installed on OMEGA almost perpendicular to the existing KBframed diagnostic: the single-line-of-sight, time-resolved x-ray imager (SLOS-TRXI). SLOS-TRXI is the product of a joint project with General Atomics (GA), Sandia National Laboratories (SNL), Kentech Instruments, Lawrence Livermore National Laboratory (LLNL), and the Laboratory for Laser Energetics (LLE). It comprises a new generation of fast-gated x-ray framing camera that is capable of capturing multiple frames along a single line of sight with $\sim 40\text{-ps}$ temporal resolution and high spatial resolution. It captures x-ray images of the core of an imploded target during high-energy-density (HED) physics experiments for analysis.

Figure 154.21 shows a schematic of SLOS-TRXI in its initial configuration. The x-ray-emitting hot spot is imaged with a pinhole onto a photocathode through several foil filters that protect the diagnostic from target debris, optical emission, and contamination. A fraction of the photons is absorbed in the photocathode, producing secondary photoelectrons. The photoelectron image is then imaged with 1:1 magnification through a 75-cm-long drift tube containing a homogenous magnetic field of 6 kG onto a nanosecond-gated, burst-mode, hybrid complementary metal-oxide semiconductor (hCMOS) sensor developed by SNL.⁴ SLOS-TRXI uses the radiation-tolerant system Icarus IIG6 (Ref. 5), which was developed for the National Ignition Facility (NIF).⁶ The novel aspect is to combine the electron pulse-dilation imager technique^{7,8} developed by GA and LLNL with a nanosecond-gated hCMOS sensor. A temporally varying voltage is applied between the photocathode and a grid that accelerates the photoelectrons to a speed that depends on the time when they are produced by the x rays. The kinetic energy of early photoelectrons is higher than that of later electrons. The long drift tube stretches the electron pulse by a factor of ~ 70 in time because of the different times of flight. The electrons are then directly detected with the gated hCMOS sensor. The pulse-dilation technique makes it possible to achieve $\sim 40\text{-ps}$ time resolution with 2-ns gating in



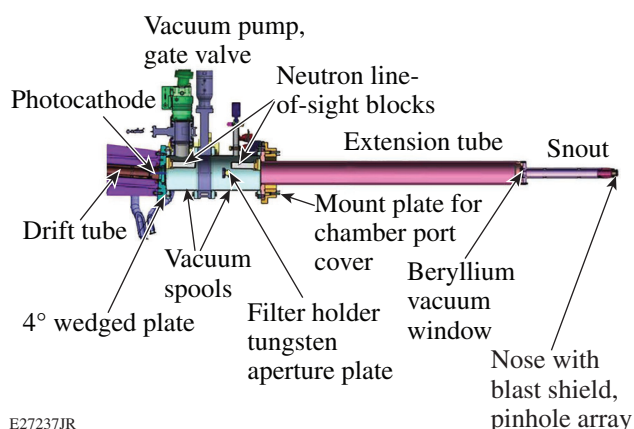
E27234JR

Figure 154.21 Schematic of the single-line-of-sight, time-resolved x-ray imager on OMEGA in its initial configuration. A pinhole is used to image the x rays from the hot spot onto a photocathode. A pulse-dilation tube stretches the secondary electron pulse in time and forms an image of the hot spot on a time-gated, solid-state detector (hCMOS). The pinhole will later be replaced with an advanced optic to provide improved spatial resolution.

the hCMOS. Efforts are underway to develop an hCMOS sensor with ~ 1 -ns gating time, which then would improve the time resolution to ~ 20 ps using the same time magnification. The combination of these two transformative technologies leads to a new class of radiation-hardened x-ray imagers that will have a significant impact in HED diagnostic applications requiring high temporal and spatial resolutions on the NIF,⁶ Sandia's Z machine,⁹ and OMEGA.³

Mechanical Design of the Pinhole Imager

Figure 154.22 shows a computer-aided design (CAD) model of the front part of SLOS-TRXI. The snout comprises a pinhole-array imager casting multiple images of the hot spot onto the detector. The pinhole array with $10\text{-}\mu\text{m}$ -diam holes is placed 166.5 mm from target chamber center (TCC), where the imploding target is located. The pinhole array is sandwiched between two $500\text{-}\mu\text{m}$ -thick Ta collimators with $150\text{-}\mu\text{m}$ -diam holes and is protected from target debris by a $254\text{-}\mu\text{m}$ -thick Be-foil blast shield. The hole spacing in the collimators and the pinhole array is 238 ± 5 μm in the vertical and 381 ± 5 μm in the horizontal directions. Collimators and the pinhole array are mounted in a spring-loaded nose cap, which can be easily changed during a vacuum chamber entry. A second $254\text{-}\mu\text{m}$ -thick Be foil between the snout and the extension tube serves as a vacuum window and separates the clean, high vacuum on the detector side from the target chamber vacuum. The CsI photocathode is located 2238 mm from TCC, providing a spatial magnification of 12.4 . A tungsten aperture is located 1904 mm from TCC to reduce background from scattered radiation. An image plate with a rectangular opening can be placed in front of the aperture to obtain additional time-integrated pinhole images of the implosion. The spatial



E27237JR

Figure 154.22
CAD model of the pinhole imager that produces an x-ray image on the photocathode of SLOS-TRXI.

magnification for the images on the image plate is 10.4 . A gate valve is placed between the two vacuum spools, allowing one to change the image plate between shots without breaking the vacuum in the drift tube. The drift tube is tilted by 4° in the vertical direction, thereby moving the hCMOS sensor out of the direct line of sight of radiation from the target. The main reason for this adjustment is to prevent neutron-induced background in high-yield shots from compromising the signal. Two 100-mm -thick blocks of polyethylene, each encapsulated in a stainless-steel case, were placed in the direct line of sight to reduce the neutron flux on the hCMOS sensor.

SLOS-TRXI is installed in the H4F port (polar angle of 45.2° and azimuthal angle of 234°) of the OMEGA target chamber. Figure 154.23 shows the installation of the diagnostic on OMEGA. The x-ray imager, located inside the target chamber, is not visible. The long aluminum housing contains the pulse dilation tube, the hCMOS detector, and various electronic components.

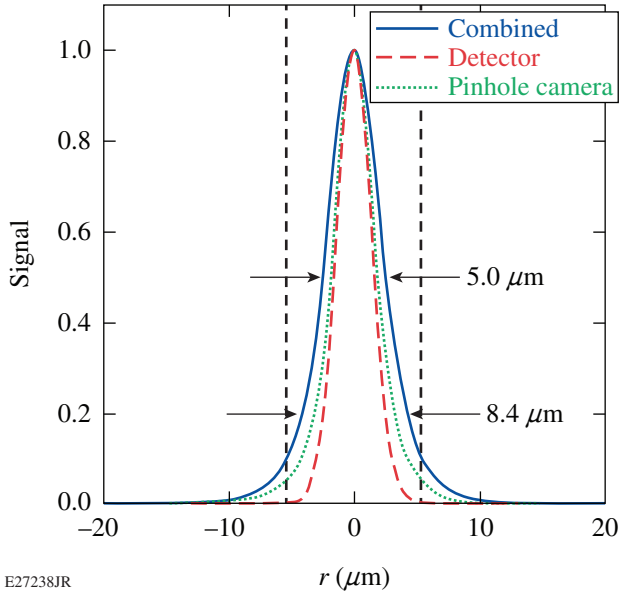


E27245JR

Figure 154.23
Installation of the SLOS-TRXI diagnostic on the OMEGA target chamber.

Figure 154.24 shows the calculated point-spread function (PSF) of the diagnostic (solid blue curve) in the target plane, which was obtained by convolving the pinhole imager PSF (dotted green curve) with the detector PSF (dashed red curve). The pinhole PSF was calculated for a pinhole diameter of 10 μm using the Fresnel approximation and spectrally averaging over the calculated spectral response for a cryogenic target implosion on OMEGA (see Fig. 154.27, p. 84). The detector PSF was assumed to be of Gaussian shape with a full width at half maximum (FWHM) of 40 μm in the image plane based on the Larmor radius of the electrons in the magnetic field inside the drift tube and a pixel size of 25 μm in the hCMOS

sensor. The corresponding detector width in the target plane is $3.2 \mu\text{m}$ by taking the spatial magnification into account. The calculated FWHM of the convolved diagnostic PSF is $5.0 \mu\text{m}$ and the full width at the 20% point is $8.4 \mu\text{m}$. The two vertical dashed lines mark the $10.7\text{-}\mu\text{m}$ calculated spatial resolution of the pinholes from geometrical optics. Dedicated shots that will measure the spatial resolution of the diagnostic are planned.



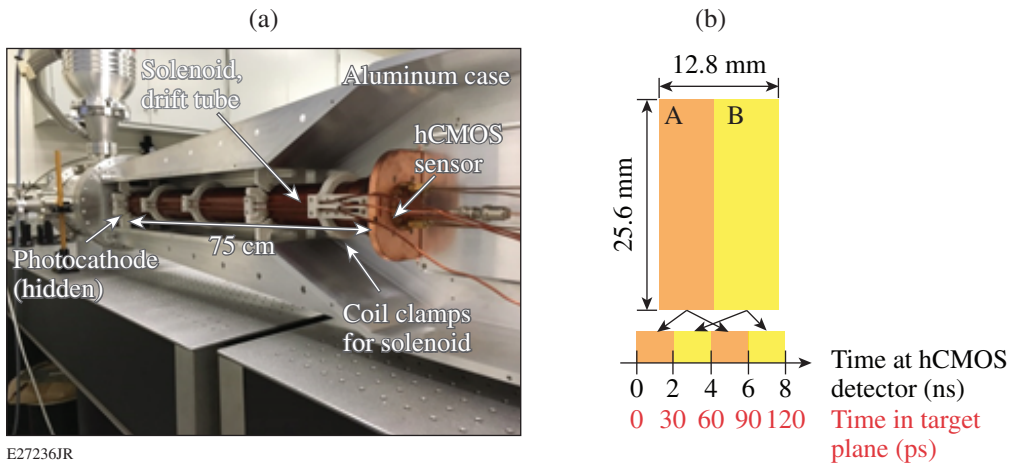
E27238JR

Figure 154.24
Calculated point-spread function (PSF) of the pinhole imager (dotted green curve), the detector PSF (dashed red curve), and the combined PSF (solid blue curve).

The pinhole imager will be replaced later in phase II with an advanced optic to provide improved spatial resolution.

Drift Tube and Hybrid Complementary Metal-Oxide Semiconductor Detector

Figure 154.25(a) shows the back part of SLOS-TRXI on a test bench with the solenoid-wound drift tube and hCMOS sensor at the right end, installed in their aluminum housing. The inside of the drift tube and the sensor are at vacuum; the electronics and the case are in air. The electronics include a magnet pulser, capacitors, and a photocathode pulser that are stored in the back of the aluminum case (not shown in the figure). Two energy storage capacitors generate a 6-kG magnetic field at the photocathode. Figure 154.25(b) shows a schematic of the hCMOS sensor and its timing. The sensor is comprised of 1024×512 pixels with a size of $25 \mu\text{m} \times 25 \mu\text{m}$, providing a total detector area of $25.6 \text{ mm} \times 12.8 \text{ mm}$. It is split into two halves (hemisphere A and hemisphere B) that can be independently gated to provide continuous temporal coverage. The reading sequence is frame 1 (A,B) and frame 2 (A,B). The schematic shows how each hemisphere is timed. The black time axis corresponds to time at the hCMOS detector, which shows that each hemisphere is alternatively read out with an integration time of 2 ns and a 2-ns delay between hemispheres, providing a total of four snapshots. The red time axis is the effective instrument time at the target plane when taking the time magnification of the pulse-dilation drift tube into account. The available time range covers $\sim 120 \text{ ps}$. Each hemisphere provides a sufficient area to accommodate multiple



E27236JR

Figure 154.25
(a) Photograph of the solenoid with a drift tube and hCMOS sensor installed in the aluminum case. The camera is mounted on a test bench for testing. The space on the right is for electronics that include a magnet pulser, capacitors, and a photocathode pulser (not shown). (b) Schematic of the timing of the hCMOS sensor. The black time axis corresponds to time at the hCMOS detector, while the red time axis corresponds to time at the target plane for maximum time magnification because of the pulse dilation in the drift tube.

images of the hot spot. The images of each hemisphere that are simultaneously read out can then be added up to improve signal fidelity and signal-to-noise ratio. Another possibility is to apply different filtration across different regions of the sensor to obtain hot-spot images for different photon-energy ranges and to improve the dynamic range.

The temporal resolution and gate profiles of SLOS-TRXI were measured using a pulsed UV laser with a pulse duration of 21-ps FWHM and a wavelength of 266 nm. The laser beam was focused to a single 1-mm-diam FWHM spot onto the photocathode, and an image formed in the center of one of the hCMOS hemispheres. Separate scans for each hemisphere were obtained by shifting the laser spot on the other hemisphere. The gate-width scan consists of 100 image captures as the relative timing of the laser pulse and the SLOS-TRXI gate was varied in 2-ps steps. The system's trigger jitter was ~ 25 ps. A fast oscilloscope measured simultaneously the monitor pulse from the photocathode and the laser pulse to remove the jitter and to obtain high-fidelity temporal profiles. The laser pulse width and the detector gate width are about the same so deconvolution was needed to infer true gate width. Gate-width scans were taken at various laser intensities to measure space-charge broadening of the electron pulse. Figure 154.26 depicts the measured effective gate profiles. The sensor was operated in (2,2) mode with a delay of 2 ns and the drift tube at nominal $80\times$ temporal magnification, which is currently the fastest performance mode for SLOS-TRXI with the Icarus 1 sensor.

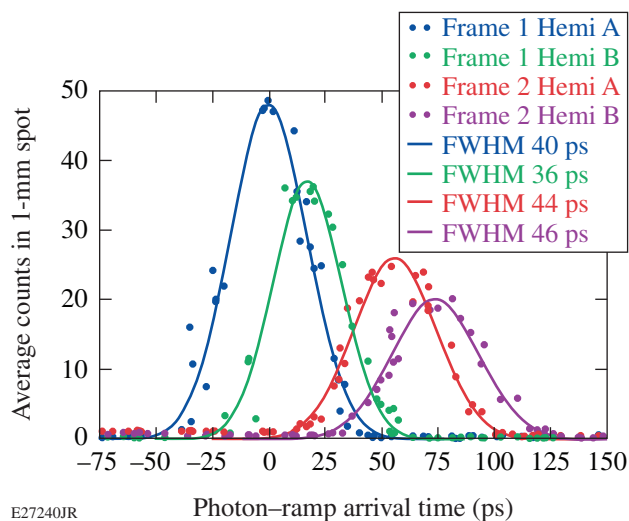


Figure 154.26
Measured gate profiles of the four frames in (2,2) mode with a delay of ~ 2 ns and nominal $80\times$ temporal magnification. The gate width varies from 36 to 46 ps.

The frame-to-frame amplitude decay is caused by an electron energy drop during ramp and a lower detection efficiency of the hCMOS for lower-kinetic-energy photoelectrons produced later in time. The laser intensity was chosen to give 20% space-charge broadening of the electron pulse in frame 1, which effectively lowers the temporal magnification from nominally $80\times$ to $\sim 70\times$. The solid curves are fits with a Gaussian-shaped curve to the data and the corresponding FWHM's are given in the legend. The effective gate FWHM varies from 36 to 46 ps and the sensitivity drops by about a factor of 2. The system operation is quite stable. Space-charge broadening increased with the laser intensity, which resulted in longer gate widths. Further details on the electron detection by the hCMOS sensor and the drift-tube design, its operation, and characterization can be found in Ref. 10.

Activation Shots on OMEGA

A series of activation shots were taken, and the diagnostic was used for the first time on cryogenic target implosions in September 2017. In its initial phase, the imaging concept was tested under the high background from neutrons and hard x rays in OMEGA cryogenic target implosions. The experiment used 60 UV ($\lambda = 351$ nm) beams from the OMEGA laser³ with an energy of up to 28 kJ. The diagnostic has been successfully activated with (1) flat-foil shots with dedicated beams, (2) room-temperature exploding-pusher implosions of thin glass shells with various fills (DT and D_2 with Ar dopant),¹¹ and (3) cryogenic implosions with 42- μm -thick DT ice targets providing neutron yields of up to $\sim 1 \times 10^{14}$ (Ref. 12). Coarse timing within ~ 200 ps was achieved in the first campaign at lower temporal resolution (~ 250 ps). Fine timing within ~ 50 ps was achieved in the second and third campaigns with higher temporal resolution (~ 40 ps). Figure 154.27 shows the detected spectrum of SLOS-TRXI for an OMEGA cryogenic target implosion from a photometric calculation. The calculation used the spectrum from a 1-D hydrodynamic simulation (obtained with the code *LILAC*¹³) of a cryogenic target, the solid angle of the pinhole imager, an integration time of 30 ps, the transmission through 508 μm of Be, 51 μm of Kapton (the photocathode substrate), and an additional 12 μm of Cu that had to be inserted to reduce the signal level in the cryogenic shots. The calculation also considers the photon absorption in the 200-nm-thick CsI photocathode layer. The detected spectrum ranges from 4 to 9 keV and peaks at 6 keV.

Figure 154.28 shows the core emission from cryogenic target implosion shot 87024. The instrument recorded the hot-spot x-ray emission in the photon energy range from ~ 4 to 9 keV in four frames. Each frame was integrated over ~ 40 ps and

the frame-to-frame delay time was ~ 25 ps. Up to eight pinhole images were averaged for each frame to improve the signal fidelity. The bang time was in the fourth frame showing the smallest object. The data show that shots with neutron yields of up to 1×10^{14} produced no neutron-induced background in the

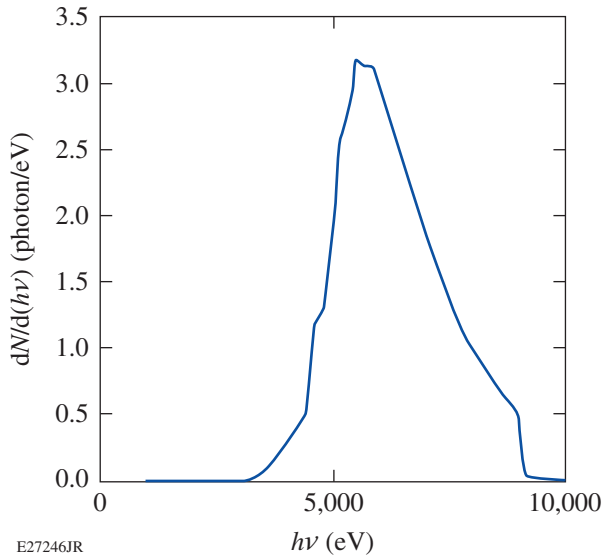


Figure 154.27
Detected spectrum of SLOS-TRXI for an OMEGA cryogenic target implosion from a photometric calculation.

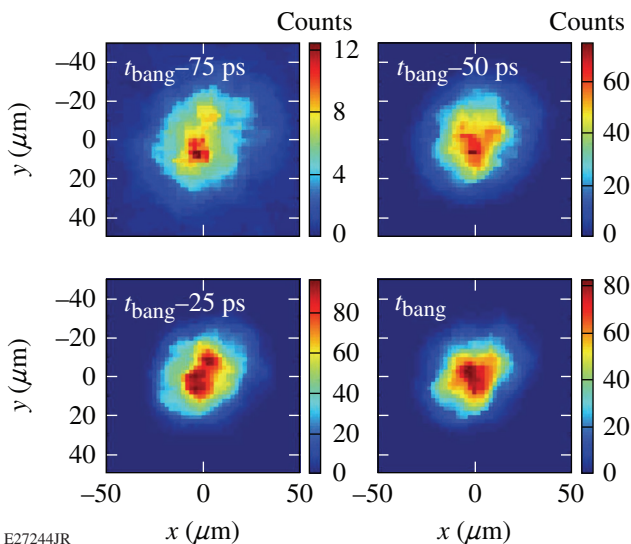


Figure 154.28
Four frames of the hot-spot x-ray emission (~ 4 to 9 keV) were recorded in cryo shot 87024 with the bang time in the fourth frame. For each frame multiple pinhole images were averaged in order to improve the signal fidelity.

hCMOS. Space-charge effects currently dictate that the signal level of the instrument is kept below 100 counts per pixel. With a noise floor of one count per pixel, this limits the dynamic range to two orders of magnitude.

The pattern from the pinhole array provides an *in-situ* measure for the image magnification. Eddy currents in the aluminum case surrounding the drift tube cause a slight anamorphic demagnification when imaging the photoelectrons from photocathode to hCMOS. The design magnification of $12.4\times$ is slightly reduced to $11.9\times$ in the vertical and $11.4\times$ in the horizontal direction. The images were warp corrected by rotating and scaling in x and y to minimize residual error between fitted centroids of each image and the pinhole array centers. The drift tube contains three grids with a period of $230 \mu\text{m}$. The grid structure becomes visible in the hot-spot image at high signal levels, which affects to some extent the quality of a single pinhole image and the signal-to-noise ratio. The grid structure averages out when overlapping multiple pinhole images. In the future this will be mitigated by using grids with a larger period so there is less interference with the spatial structures that are imaged.

Conclusions

The single-line-of-sight, time-resolved x-ray imager (SLOS-TRXI) has been activated on OMEGA to provide time-resolved images of the core of imploded cryogenic deuterium–tritium shells in inertial confinement fusion experiments. Activation shots with neutron yields of up to 1×10^{14} produced background-free images of the imploded core in four frames. In phase II, the diagnostic will be further developed to improve the spatial resolution, add additional frames, achieve a higher space-charge operating limit, and provide better temporal resolution. Advanced x-ray optical systems that are under consideration include a Kirkpatrick–Baez optic, a Wolter-like optic, and penumbral imaging.

ACKNOWLEDGMENT

This work was supported by the DOE NNSA under awards No. DE-NA0001944 and DE-FC02-04ER54789, the Laboratory Basic Science Program, the University of Rochester, and the New York State Energy Research and Development Authority.

REFERENCES

1. S. P. Regan, V. N. Goncharov, I. V. Igumenshchev, T. C. Sangster, R. Betti, A. Bose, T. R. Boehly, M. J. Bonino, E. M. Campbell, D. Cao, T. J. B. Collins, R. S. Craxton, A. K. Davis, J. A. Delettrez, D. H. Edgell, R. Epstein, C. J. Forrest, J. A. Frenje, D. H. Froula, M. Gatu Johnson, V. Yu. Glebov, D. R. Harding, M. Hohenberger, S. X. Hu, D. Jacobs-

- Perkins, R. T. Janezic, M. Karasik, R. L. Keck, J. H. Kelly, T. J. Kessler, J. P. Knauer, T. Z. Kosc, S. J. Loucks, J. A. Marozas, F. J. Marshall, R. L. McCrory, P. W. McKenty, D. D. Meyerhofer, D. T. Michel, J. F. Myatt, S. P. Obenshain, R. D. Petrasso, R. B. Radha, B. Rice, M. Rosenberg, A. J. Schmitt, M. J. Schmitt, W. Seka, W. T. Shmayda, M. J. Shoup III, A. Shvydky, S. Skupsky, A. A. Solodov, C. Stoeckl, W. Theobald, J. Ulrich, M. D. Wittman, K. M. Woo, B. Yaakobi, and J. D. Zuegel, *Phys. Rev. Lett.* **117**, 025001 (2016); **117**, 059903(E) (2016).
2. F. J. Marshall, R. E. Bahr, V. N. Goncharov, V. Yu. Glebov, B. Peng, S. P. Regan, T. C. Sangster, and C. Stoeckl, *Rev. Sci. Instrum.* **88**, 093702 (2017).
 3. T. R. Boehly, D. L. Brown, R. S. Craxton, R. L. Keck, J. P. Knauer, J. H. Kelly, T. J. Kessler, S. A. Kumpan, S. J. Loucks, S. A. Letzring, F. J. Marshall, R. L. McCrory, S. F. B. Morse, W. Seka, J. M. Soures, and C. P. Verdon, *Opt. Commun.* **133**, 495 (1997).
 4. L. Claus, *et al.*, *Proc. SPIE* **9591**, 95910P (2015).
 5. A. C. Carpenter *et al.*, *Proc. SPIE* **9966**, 99660H (2016).
 6. E. M. Campbell and W. J. Hogan, *Plasma Phys. Control. Fusion* **41**, B39 (1999).
 7. R. D. Prosser, *J. Phys. E: Sci. Instrum.* **9**, 57 (1976).
 8. T. J. Hilsabeck *et al.*, *Rev. Sci. Instrum.* **81**, 10E317 (2010).
 9. R. B. Spielman, W. A. Stygar, J. F. Seamen, F. Long, H. Ives, R. Garcia, T. Wagoner, R. W. Struve, M. Mostrom, I. Smith, D. Spence, and P. Corcoran, in *11th IEEE International Pulsed Power Conference*, edited by G. Cooperstein and I. Vitkovitsky (IEEE, Piscataway, NJ, 1997), Vol. 1, pp. 709–714.
 10. K. Engelhorn, T. J. Hilsabeck, J. D. Kilkenny, D. Morris, T. M. Chung, A. K. L. Dymoke-Bradshaw, J. D. Hares, P. Bell, D. Bradley, A. C. Carpenter, M. Dayton, S. R. Nagel, L. Claus, J. Porter, G. Rochau, M. Sanchez, S. P. Regan, C. Sorce, and W. Theobald, “Subnanosecond Single Line-of-Sight X-Ray Imagers,” submitted to *Review of Scientific Instruments*.
 11. M. J. Rosenberg, H. G. Rinderknecht, N. M. Hoffman, P. A. Amendt, S. Atzeni, A. B. Zylstra, C. K. Li, F. H. Séguin, H. Sio, M. Gatu Johnson, J. A. Frenje, R. D. Petrasso, V. Yu. Glebov, C. Stoeckl, W. Seka, F. J. Marshall, J. A. Delettrez, T. C. Sangster, R. Betti, V. N. Goncharov, D. D. Meyerhofer, S. Skupsky, C. Bellei, J. Pino, S. C. Wilks, G. Kagan, K. Molvig, and A. Nikroo, *Phys. Rev. Lett.* **112**, 185001 (2014).
 12. R. Betti, J. P. Knauer, V. Gopalaswamy, D. Patel, K. M. Woo, K. S. Anderson, A. Bose, A. R. Christopherson, V. Yu. Glebov, F. J. Marshall, S. P. Regan, P. B. Radha, C. Stoeckl, and E. M. Campbell, *Bull. Am. Phys. Soc.* **62**, BAPS.2017.DPP.TI2.1 (2017).
 13. J. Delettrez, R. Epstein, M. C. Richardson, P. A. Jaanimagi, and B. L. Henke, *Phys. Rev. A* **36**, 3926 (1987).